Supplementary Information (SI) for Journal of Materials Chemistry C.

Supplementary Information for

Self-Induced MBE-grown InAsP Nanowires on Si Wafers for SWIR Applications

Andrey K. Kaveev[a,b], Vladimir V. Fedorov[*a,c], Alexander V. Pavlov[a,c], Dmitry V. Miniv[a], Demid A. Kirilenko[b,c], Alexey Nadtochiy[a,d], Alexandr S. Goltaev[a], Andrey P. Malenin[a], Ratmir V. Ustimenko[c], Danila A. Karaulov[c], Maxim Ya. Vinnichenko[c], Eduard Moiseev[d] and Ivan S. Mukhin[a,c]

[a] Alferov University, 194021 St. Petersburg, Russia

[b] Ioffe Institute, 194021 St. Petersburg, Russia

[c] Peter the Great St.Petersburg Polytechnic University, 195251 St. Petersburg, Russia

[d] HSE University Saint Petersburg, International Laboratory of Quantum Optoelectronics, 194100 St. Petersburg, Russia;

♦corresponding author e-mail: burunduk.uk@gmail.com

S1. Additional SEM images of the InAsP NW arrays.

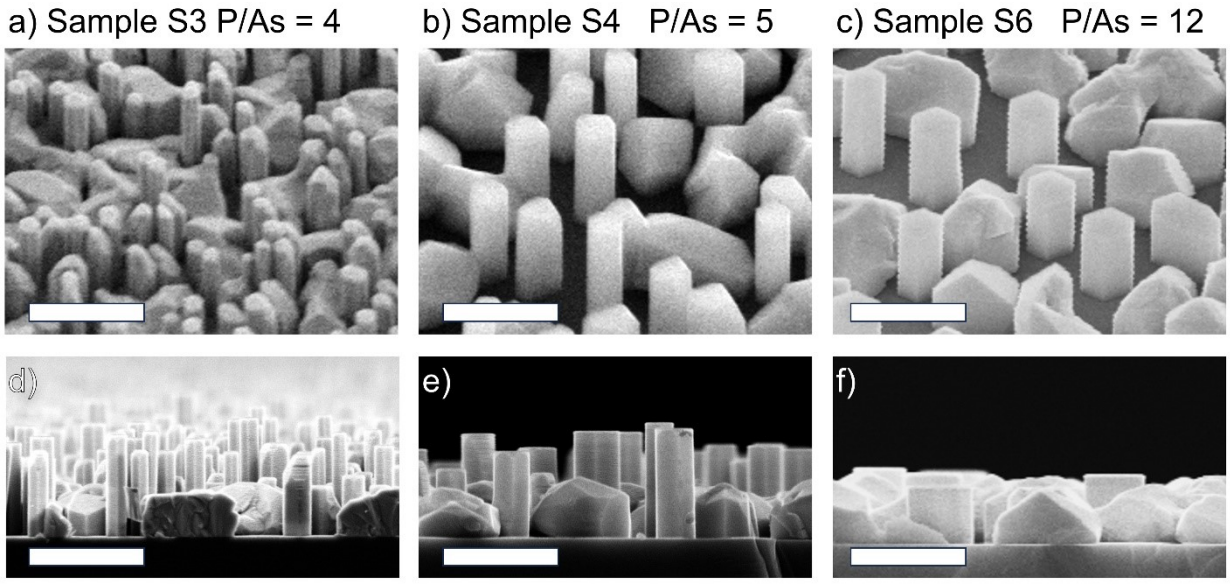

Fig. S1. The inclined (a-c) and cross-sectional (d-f) SEM images of the grown NW samples: (a,b) Sample S3 - Sample S3 - InAsP NWs grown at effective P/As flux ratio of 4; (b,e) Sample S4 - InAsP NWs grown at effective P/As flux ratio of 5; (c,f) Sample S6 - InAsP NWs grown at effective P/As flux ratio of 12. The scale bar on all images is 1 μm.

S2. RHEED pattern evolution during InAsP NW growth

Self-induced NW growth is commonly accompanied by the unwanted parasitic growth of three-dimensional (3D) islands. Fig. S2 presents a series of the reflection high-energy electron diffraction technique (RHEED) acquired in-situ during the NW growth in sample S4. At the initial growth stage (Fig. S2 b), diffraction pattern corresponds to (111)-twinned zinc-blende (ZB) structure (corresponding reflections are marked by yellow and red circles) with a barely visible diffraction spots from the wurtzite (WZ) phase. As InAs NWs grow, the ZB-phase diffraction spots fade out as the 3D islands become shadowed by the NWs. By the end of the growth, WZ diffraction spots elongated along NW growth direction in diffuse intensity streaks are observed (Fig. S2 c,d).

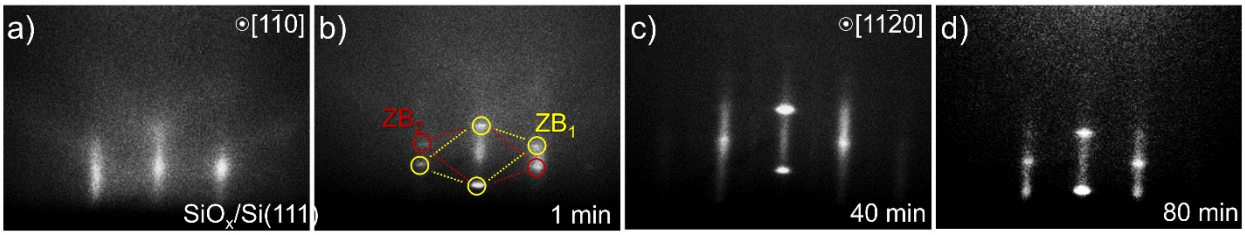

Fig. S2. RHEED patterns acquired during the growth of InAsP NWs at high P-to-As ratio in sample S4.

S3. Tentative composition analysis using SEM-EDS

The composition of NWs in the studied samples were additionally analyzed using SEM with energy dispersive X-ray spectroscopy (SEM-EDS) technique. We obtained characteristic X-ray emission maps from the cleaved edges of NW samples and analyzed the corresponding emission spectra from the NWs. InAs and InP wafers were used as references. A monotonic increase in phosphorus content in the InAsP NWs as the P-to-As ratio increases was observed. Corresponding SEM images and EDS elemental maps are presented in Fig. S3.

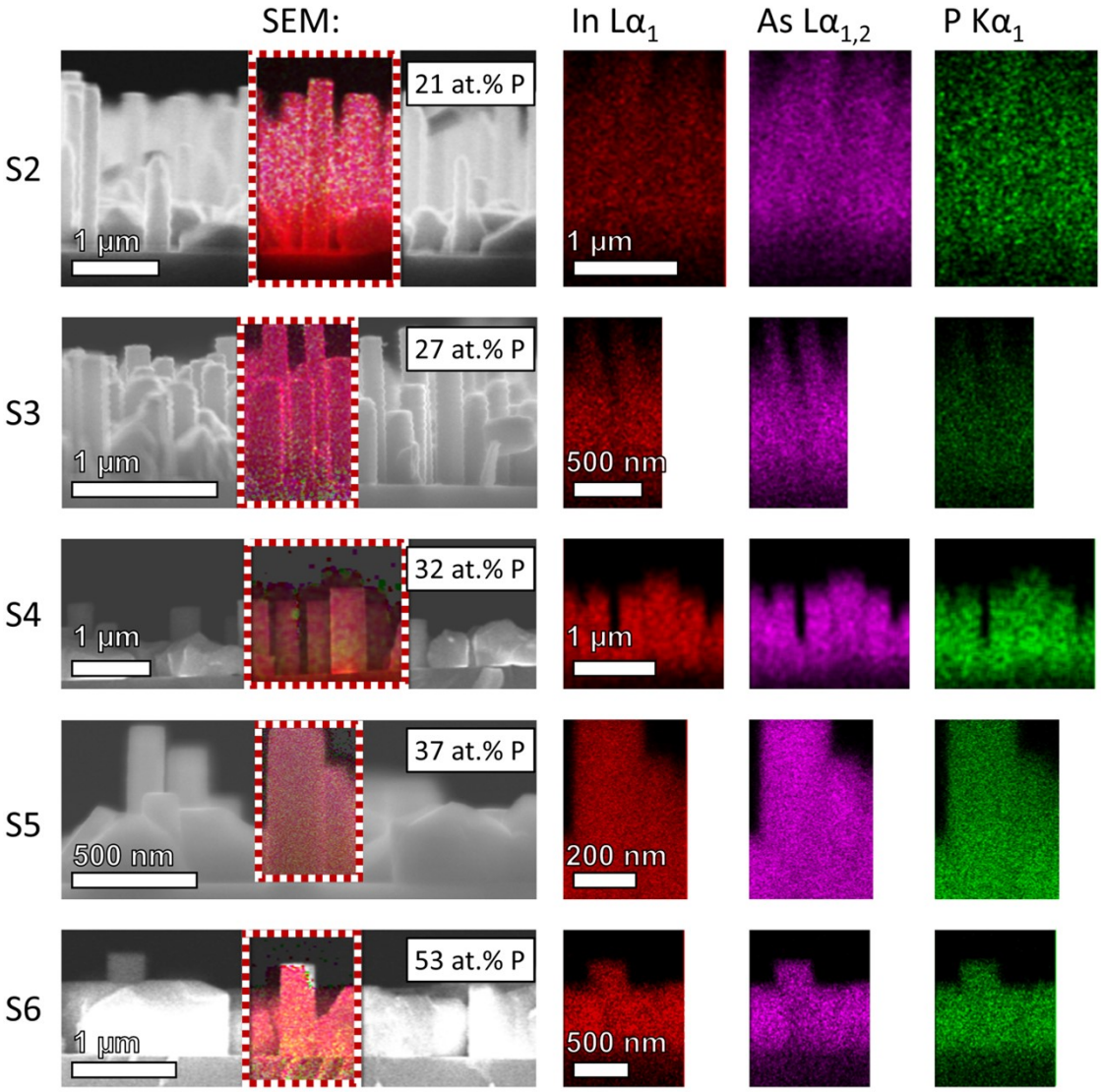

Fig. S3. Cross-sectional SEM images of the cleaved edge of NW samples with the corresponding EDS elemental maps showing the phosphorus and arsenic distribution in the NW samples. The dashed areas in the left panel show the region of EDS analysis. Each series of In $L\alpha_1$, As $L\alpha_{1,2}$ and P $K\alpha_1$ elemental maps are plotted on the same scale, with the scale bar provided on the corresponding In $L\alpha_1$ map. The estimated concentrations of P are shown in the inserts of the left panel.

S4. The reciprocal lattices of the Wurtzite and Zinc Blende phases of InAsP

Fig. S4 illustrates the relative orientation of the two-dimensional X-ray diffraction reciprocal space maps (XRD-RSMs) and the reciprocal lattice nodes of the InAs Wurtzite (WZ) and Zinc Blende (ZB) phases within the $<11\text{-}20>_{WZ}$ and $<1\text{-}10>_{ZB}$ zero order Laue zones (ZOLZ) of corresponding structures. The representation adheres to the following constraints: (1) in-plane and out-of-plane scattering vectors takes positive values ($Q_{in\text{-}plane}>O$, $Q_{out\text{-}of\text{-}plane}>O$), and (2) maximum values of scattering vector is limited by the Cu Kα wavelength: $Q_{max}<2/\lambda_{Cu\ K\alpha}$. It is evident that the (4-403) Bragg reflection of the WZ phase does not coincide with the reciprocal lattice nodes of the ZB phase. Consequently, the contributions from the WZ and ZB phases can be distinctly identified in the X-ray diffraction reciprocal space mapping (XRD-RSM) taken in the vicinity of the asymmetric reflections lying within the $<11\text{-}20>_{WZ}$ ZOLZ of the WZ InAsP structure.

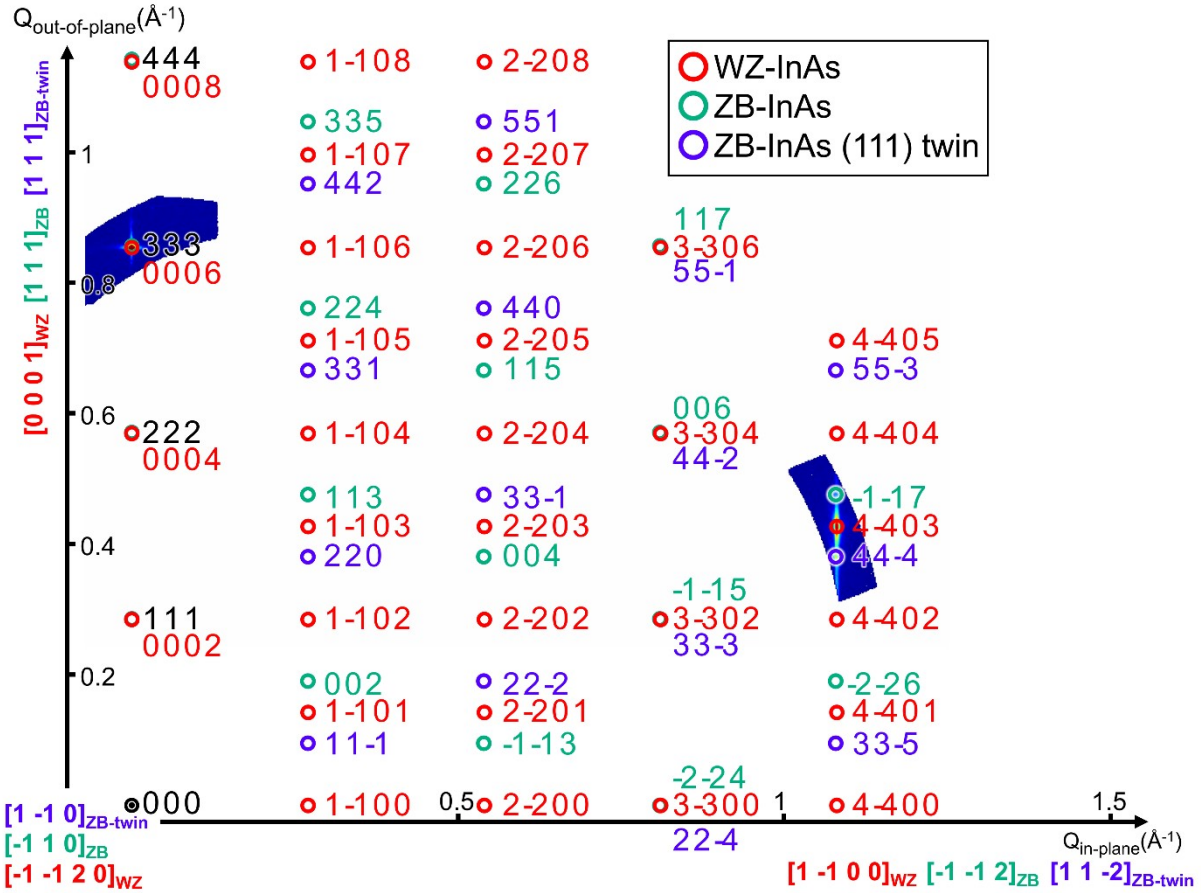

Fig. S4. First quadrant ($Q_{in\text{-}plane}$,$Q_{out\text{-}of\text{-}plane}>O$) of the $<11\text{-}20>_{WZ}$ and $<1\text{-}10>_{ZB}$ zero order Laue zones for the WZ and ZB phases of the InAs.

S5. Additional DFT data.

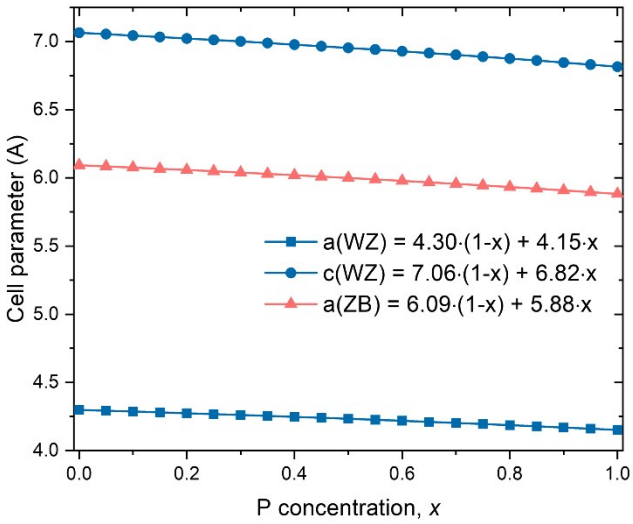

Fig. S5. The calculated cell parameters (filled symbols) for ZB and WZ InAsP cells for different P concentrations. The lines represent the approximation according to Vegard's law (see legend).

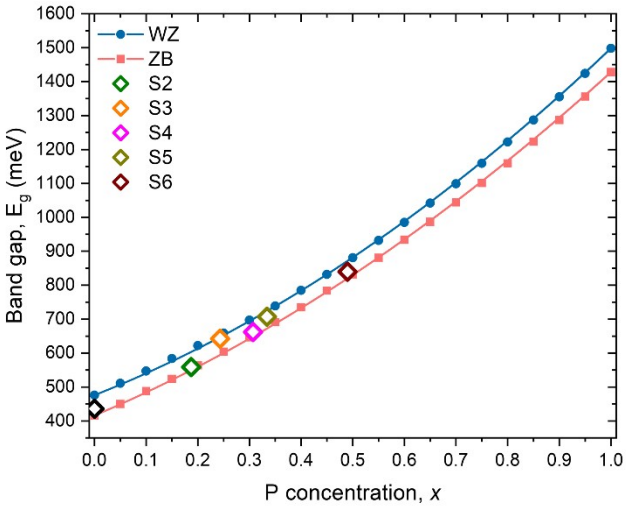

Fig. S6. The calculated cell parameters for ZB and WZ InAsP cells on P concentration.

S6. Lattice parameters and composition of the InAsP NW arrays

Sample	As/P flux ratio	a, b (Å)	c, (Å)	$InAs_{1-x}P_x$ alloy composition, x (at.%)
S1	-	4.277	7.017	0
S2	1:2	4.253	6.972	18.7
S3	1:4	4.246	6.959	24.3
S4	1:5	4.238	6.943	30.7
S5	1:6	4.235	6.935	33.4
S6	1:12	4.208	6.919	49.3

Table S1. Lattice parameters of the WZ InAs and InAsP NW according to the XRD-RSM analysis. InAsP alloy composition derived from Vegard's law for samples S2-S6.

S7. Raw RT photoluminescence data.

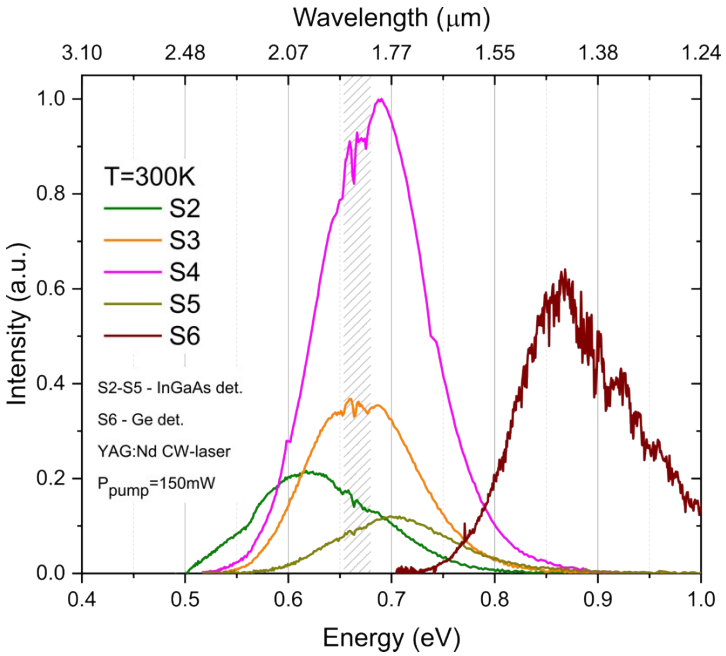

Fig. S7. RT PL spectra of InAsP NWs (samples S2-S6). The spectrum for S6 was obtained using a Ge-based photodiode in contrast to the samples S2-S6 measured with an extended-range InGaAs one.The dashed area marks the position of water absorption lines. Data points corresponding to the maximum absorption of the PL signal by water vapor were excluded when smoothing the experimental data.